# Re-design of a Wind Tunnel Outflow Section

Pier Giorgio Spazzini, Riccardo Malvano, and Aline Piccato
INRIM – Italy
Strada delle Cacce, 91 – 10135 Torino (Italy)
Contact Author: P.G. Spazzini - +39 011 0906862/+39 011 0906859. p.spazzini@inrim.it

**Abstract:** This paper deals with some of the problems connected with the design of a wind tunnel. In particular, the flow in the diffuser is analyzed in detail. The tool for this analysis was the numerical simulation, which allowed to forecast possible problems and to set up strategies to overcome them before the device was built. The simulations required to reach this aim will be presented, alongside with the results obtained. The results will be discussed in the light of the objectives of the device, which is designed to improve the performance of a reference test rig for airspeed measurement.

**Keyword:** wind tunnel – airspeed – CFD for metrology – flow separation

## 1. Introduction

The measurement of airspeed is a sector of metrology which is gaining increasing importance as more and more industries submit requirements for referable anemometers.
The classical test rig to be used for the calibration of anemometers is a wind tunnel. The most important parameters for a wind tunnel used as a standard for airspeed are connected to the flow field qualities; specifically, it is important that the flow is stable and uniform across the wind tunnel test chamber. Another important parameter to be considered is the direction of the main flow, as several types of anemometers are sensitive to the flow direction. It is therefore desirable that the flow misalignment with respect to the wind tunnel axis is kept within well-defined limits.
The airspeed standard at I.N.Ri.M. is defined through a set of four test rigs, two of which (dragging test rigs) were described in recent papers [4,6]. The other two test rigs are two wind tunnels, one of which is being renovated. In particular, the part of the tunnel downstream of the test chamber, which includes the fan, the engine and the divergent presently used will be replaced with a new build which is expected to allow better performances, particularly regarding the uniformity and regularity of the flow. The general design of the new part will be a re-adaptation of the original design, see Section 2. In order to clarify the reasons for some design choices and to assess which elements were essential for the appropriate functioning of the device, some CFD simulations were performed about the divergent section.
The present flow field situation within the wind tunnel was presented in a previous paper [5]; these data are important as, alongside with analogous data to be measured after the upgrade will be completed, they will allow to assess the improvement actually obtained. In the present paper, a series of numerical simulations performed about the renovated divergent will be presented, alongside with a discussion of their meaning and the expected impact on the test rig performance.

## 2. Test Rig Description

The test rig described in the present work (Fig. 1), together with other test rigs at INRIM, forms the Italian National Standard for airspeed; it is used for the calibration of small and medium sized anemometers for airspeeds up to 25 m/s.
The test rig consists of an open-circuit, semi-open test chamber wind tunnel. The test chamber is contained within a closed parallelepiped with transparent walls, and a size of 0.90 x 0.90 x 0.97

m3. The flow in the test chamber is a free jet within this parallelepiped, with an initial diameter of 0.4 m and an available length of about 0.5 m. The propeller is downstream of the test chamber, hence the flow is sucked in. The tunnel was first built in the thirties under design by Proff. C. Ferrari and M. Panetti [2, 3]. A few years ago, the wind tunnel no more in safe working conditions, so it was reconditioned. In particular, the divergent and the engine/propeller group were replaced by a fan in a slowly diverging tube. The simplified design was adopted because of budget constraints. The renewed rig has a satisfactory behaviour in the lower part of its range, but when the velocity is increased, it undergoes strong vibrations induced by the flow. This fact, is strongly undesirable as it affects the precision of the measurements in the higher part of the range and, in the long run, might affect the integrity of the test rig itself. Therefore the divergent and engine/propeller parts of the wind tunnel are being reviewed again, using a design inspired to the original one. In the present paper, we will present the CFD analysis that was performed on the new divergent in order to validate the design concepts and evaluate possible simplifications of the configuration adopted. The range of the wind tunnel is from 0 to 25 m/s but it is referable only between 2.0 and 25.0 m/s. The reference airspeed is obtained through the measurement of the pressure drop across the convergent; the airspeed is computed using Bernoulli's relationship and the calibration law of the tunnel:

$$V = \sqrt{\frac{2 \cdot q}{\rho_a}} = \sqrt{\frac{2 \cdot K_{Pitot} \cdot K_G \cdot \Delta p_{ring}}{\rho_a}} \qquad (1)$$

where:

- $q$ is the dynamic pressure in the test chamber;
- $K_{Pitot}$ is a correction coefficient of the Pitot tube used for the tunnel calibration;
- $K_G$ is the calibration coefficient of the wind tunnel;
- $\Delta p_{ring}$ is the pressure drop;
- $\rho_a$ is the air density.

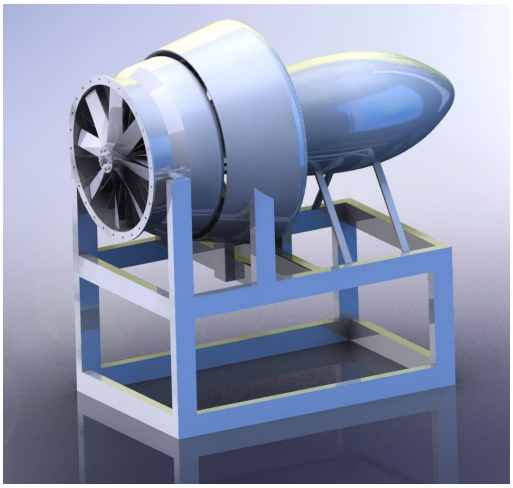

*Fig. 2.1: 3-D CAD rendering of the future wind tunnel divergent*

## 3. Numerical Simulations

The numerical simulations were performed using the STAR-CCM+ code by CD-ADAPCO [7]. Two sets of simulations of increasing complexity were performed. The first set (simpler simulations) allowed to test a larger number of configurations and therefore to quickly choose the configuration for the actual tunnel setup. The more complex simulations were run only on the

baseline configuration and on one of the others, considered as representative of all the discarded ones. The simulated field included the whole outflow region of the wind tunnel, i.e. downstream of the fan. Though, some simplifications were introduced to keep the computational cost down to a manageable level. First of all, the effect of the fan was considered to be only an increase of the flow axial velocity, i.e. the swirl and the pulsation (due to the finite number of blades) were neglected. Also, the geometry was considered to be a perfect circular section with the profile of a typical section. In the reality, some beams will connect the external parts to the engine careening. Though, these simplifications were considered to be relatively unharmful to the final result because they would not have a large influence of the flow.

### 3.1 Configurations

The main difference between the two sets of computations is in the dimension of the computational domain. The simpler set was computed on a two-dimensional domain by introducing the hypothesis of axial symmetry; the second group of simulations was performed on fully three-dimensional domains. The latter were obtained by partial rotation of the two-dimensional domain used in the first group, hence also in this case there is an underlying assumption of axially symmetrical geometry; though, the three dimensionality of the computation allows to keep into account distortions of the flow in the third direction and three-dimensional instabilities. It can be objected (see Fig. 2.1) that the actual geometry of the divergent is not fully axisymmetric; though, such asymmetries arise in the later part of the structure, where the flow unsteadiness (see Section 4) has already developed.
The three-dimensional simulations were performed mainly with the aim of checking that the results of the axially symmetrical runs were representative of the flow field in a more complex situation; as will be shown in Sec. 4, it was found out that this is indeed the case.

### 3.2 Axially symmetric cases

Several test cases were computed using this simplified model. First of all, the baseline configuration of the divergent was simulated (run 1.1). Such configuration was chosen based on the original divergent design, dating back to the 1930's (see section 2). Fig. 3.1 shows the computational grid employed in this case; the symmetry axis is at the bottom of the figure. Notice the grid refinement close to the solid walls; in this case 10 prismatic layers (see [7]) were used for the simulation of the boundary layers, allowing a satisfactory definition of the high-shear region.

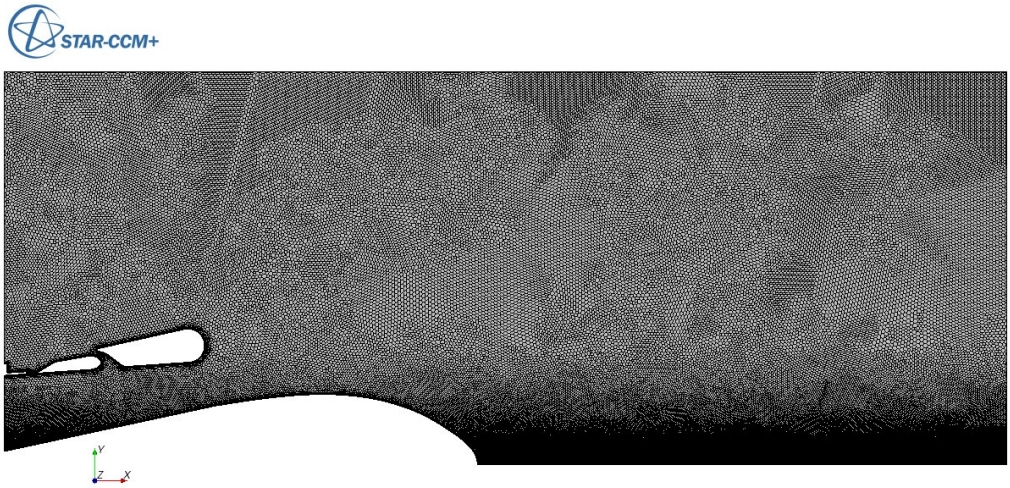


*Fig. 3.1a: Run 1.1: computational grid - overall view.*

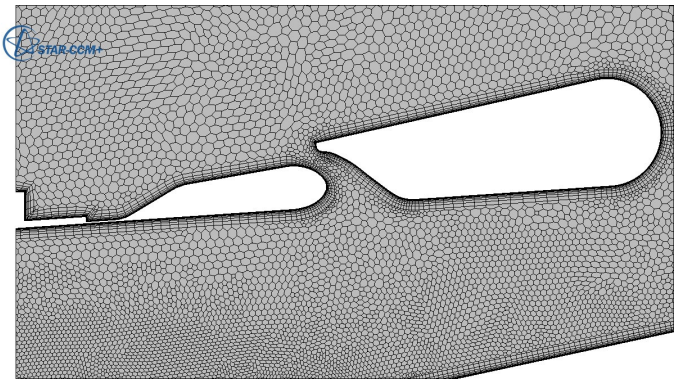

*Fig. 3.1b: Run 1.1: computational grid - detail of the diffuser.*

The total number of computational cells for this case was of approximately 115000 (polyhedral cells). The simulation was performed using a RANS method based on the $k$-$\varepsilon$ model. After this first simulation, it was decided to check the effect of the gap between the two parts of the external diffuser. Various different tests were performed to this aim (runs 1.2, 1.3a, 1.3b, 1.4a and 1.4b). Specifically, in run 1.2 the gap was grossly eliminated by inserting a solid blade in its lower part, while in the other tests the downstream part of the diffuser was moved upstream or downstream with respect to the baseline position; in runs 1.3a and 1.3b the displacement was of 20 mm upstream viz. downstream, while in test case 1.4a and b it was of 10 mm upstream/downstream. The grids employed for these tests were built with the same parameters as for run 1.1, resulting in approximately the same number of cells; also, the computations were performed using strictly the same models and parameters, in order to rule out any possible effect on the results. The extension of the simulation field was of 2 nozzle external diameters downstream of the engine careening trailing edge and of 1 nozzle external diameter in the radial direction. The field thus obtained is considered to be sufficiently large to allow the development of the relevant fluid dynamical structures without interference from the boundaries. In order to increase the computational accuracy, a second-order space discretization was used; the time discretization was performed through an implicit method, with a time step of 0.005 s.

### 3.3 Three-dimensional cases

Only two test cases were computed using this model, because of its much larger computational cost with respect to the simpler axially symmetrical cases. In particular, the two cases corresponding to runs 1.1 and 1.3b were analyzed. For coherence, these simulations will be indicated here as runs 2.1 and 2.3b. The grids for these simulations were built by considering the same extension, in the axial and in the radial direction, as in the axially symmetrical cases. Regarding the tangential extension, an opening of 45° was considered; this reduced section was chosen in order to reduce the number of cells while maintaining a sufficient grid resolution. Even so, and coarsening the grid with respect to the axisymmetric cases, a cell count of approximately 1.5 millions (polyhedral cells) was reached, which is about the limit of the computational cluster used for these computations; with this configuration, the 5-seconds simulations that will be described in section 4 required more than one week each. Although it was not possible to simulate the whole circumferential extension of the field, though, it will be shown in Sec. 4 that the constrains were sufficiently relaxed to allow the development of azimuthal instabilities. Indeed, the three dimensional grid allows a much more complete simulation of the actual situation, because it allows the generation of asymmetries within the flow. Such asymmetries

descend from small perturbations to the computation (in general caused by small inhomogeneities of the grid or by numerical errors), and are the equivalent of the asymmetries generated in real flow by small instabilities. The instabilities are then amplified because of the governing equations nonlinearities (vortex stretching phenomena), which are faithfully reproduced in the numerical simulation unless the grid is too coarse, introducing thus numerical viscosity.

## 4. Results and Comments

### 4.1 Axially symmetric cases

The results of the axisymmetric computations will first be described. Consider first of all the vorticity map reported in Fig. 4.1. It can be observed that the flow follows smoothly the engine careening (white bulk on the lower left), from which it detaches very close to the trailing

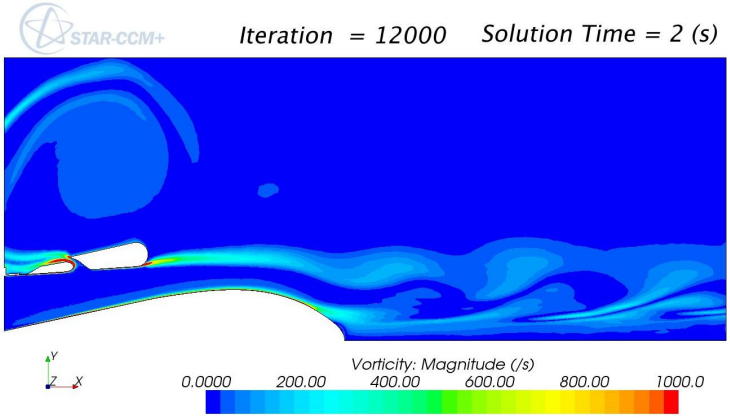


*Fig. 4.1: Run 1.1: Vorticity field at T = 2.0 s*

edge. A regular vortex shedding is also clearly observable. Notice moreover the vorticity separation at the trailing edge of the downstream part of the diffuser: observation of the time evolution of the situation showed that the position of this detachment is very stable. Analogous maps were saved at each time step, and allowed to build movies allowing to analyze the time evolution of the flow; the analysis of such movies showed that the flow field features a regular shedding of vortices of modest entity from the downstream end of the external diffuser and from the trailing edge of the careening. The expected load on the careening was also computed at every time step. The time evolution of this quantity is plotted in Fig. 4.2.

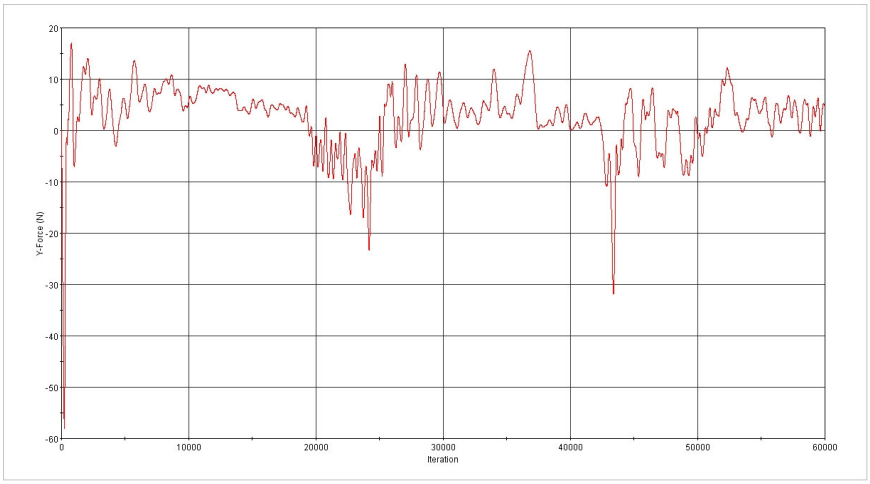


*Fig. 4.2: Run 1.1: History of vertical force on the engine careening.*

It can be observed that the history of the load exhibits very small oscillations around an average value; such oscillations can be put in relation to the vortex shedding discussed earlier. All in all, the flow in this case is very regular. The situation is strongly different when the configuration without the gap between the two parts of the diffuser (Run 1.2). Fig. 4.3 reports two vorticity maps recorded at two different instants. While in the first one the field configuration is relatively similar to the previous case (notice, though, that the regular vortex shedding observed in Fig. 4.1 is not present and that the separation at the careening trailing edge is much less smooth), at the second time instant considered the field has unstabilized and developed to a chaotic condition.

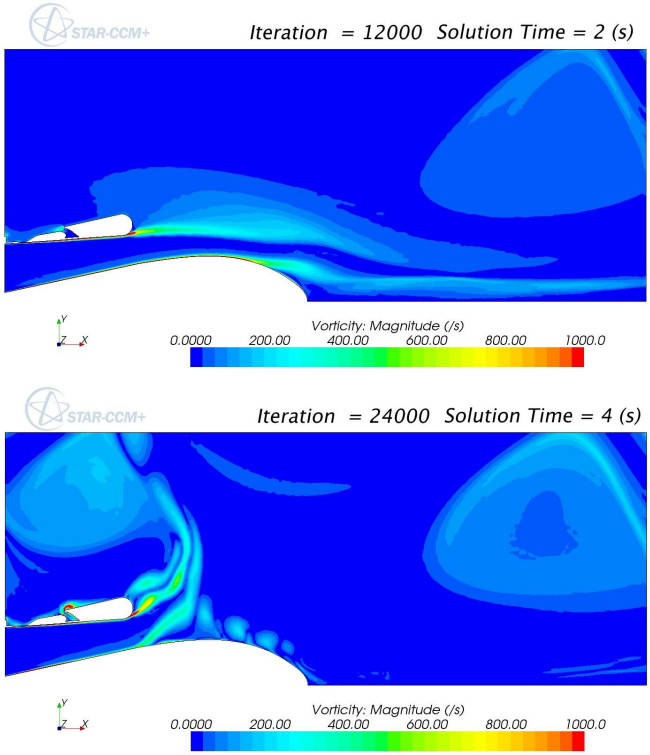


*Fig. 4.3: Run 1.2: Vorticity fields; a) T = 2.0 s; b) T= 4.0 s.*

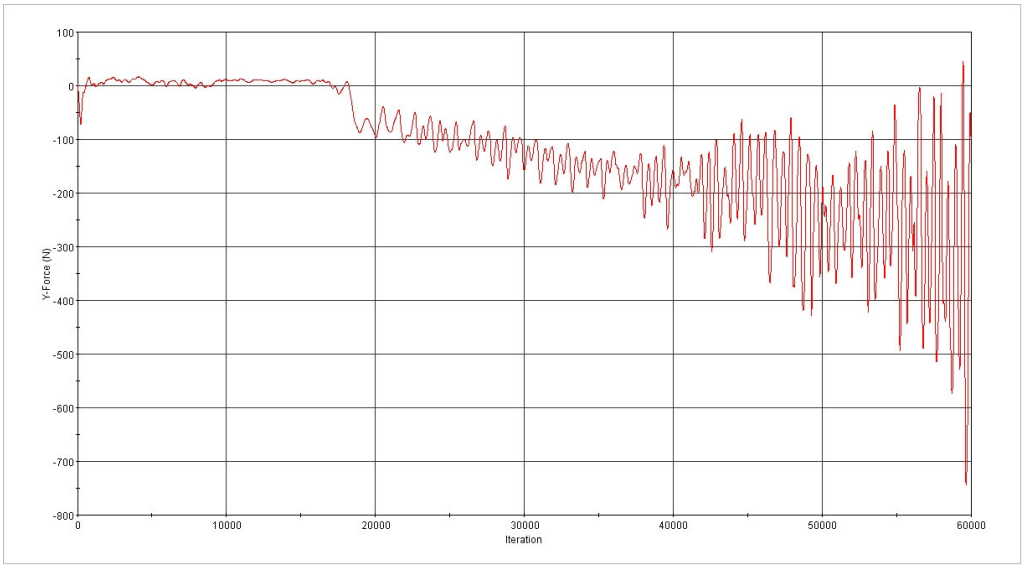


*Fig. 4.4: Run 1.2: History of vertical force on the engine careening.*

This fact is also reflected by the force history plot in Fig. 4.4, which is the counterpart of the one in Fig. 4.2. It can be observed in this figure that the fluctuation of the load on the careening is much larger. This fact indicates that the test rig, in this condition, would be subject to much larger stresses and would probably be strongly shaking and very noisy. Notice that this flow condition might not directly affect the flow in the test chamber, as the flow is still exiting the diffuser with a relatively constant mass flow rate. Though, there is little doubt that it would cause at least an increase in the turbulence level, through the shaking of the whole structure, possible fluctuating backpressures and noise. Also, the incremented mechanical stress on the test rig could harm its duration and possibly even bring to fatigue or other types of structural failure. The details of the flow field instability are presently under investigation and will be detailed in future papers, but it can be anticipated here that the main reason for this strong unsteadiness is difficulty in stabilizing the Kutta condition at the exit of the diffuser. This first result showed that the subdivision of the diffuser into two parts is essential to the correct functioning of the outflow section of the wind tunnel; the following simulations were aimed at checking the sensitivity of the flow conditions to the relative positioning of the two portions of the diffuser. First of all (Runs 1.3), the downstream part of the diffuser was displaced by 20 mm upstream and downstream with respect to the baseline position. In both cases, a chaotic flow similar to the one computed for Run 1.2 was obtained. It is interesting to observe that even the time for which the chaotic behaviour started to emerge was approximately the same as in Run 1.2, i.e. approximately 3.0 s. The preliminary analysis of the flow fields in these two cases showed that the opening of the channel between the two parts of the diffuser was, in one case so small that the circulation around the downstream part could not be established appropriately, and in the second case, made the two parts functionally independent. The analysis was then repeated (Runs 1.4) by reducing the displacement of the downstream part of the diffuser to ± 10 mm. In these cases, the flow showed a behaviour very similar to the one of Run 1.1. This brought to the somewhat surprising conclusion that the positioning of the two parts of the diffuser is a quite delicate matter, showing thus that care must be taken during the assembling of the test rig. Actually, after this result, it was decided to slightly modify the design of the mounting system of the downstream part of the diffuser in order to allow for some possibility of regulation.

### 4.2 Three-Dimensional cases

The three-dimensional computations mainly confirmed the results obtained from their 2-D counterparts. It was made clear that the origin of the phenomena described in Sec. 4.1 lies fully in the two dimensional aerodynamics.

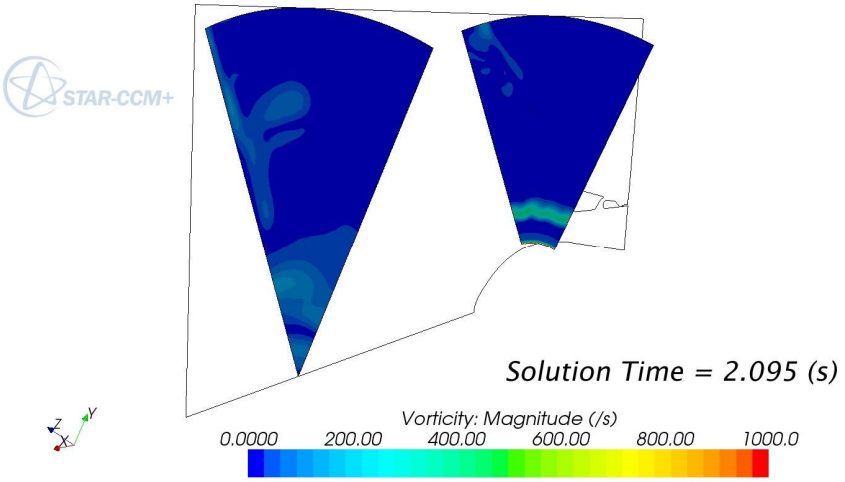


*Fig. 4.5: Run 2.3b: Map of the vorticity in two crossplanes.*

Indeed, results of Run 2.1 showed evidence of the azimuthal instabilities that are known to originate in jets, but these did not lead to the development of the global instability observed in Run 2.3b. The latter, apart from the same azimuthal instabilities developing in the jet, shows a behaviour very similar to the one of Run 1.3b. As discussed in Sec. 4.1, actually, the origin of the global instability is probably to be found in the unstable separation condition at the outlet of the diffuser. Fig. 4.5 shows a typical vorticity map in two crossplanes for Run 2.3b, before the global instability develops. It can be observed that the isovorticity contours are bent already in the first section, showing the formation of the azimuthal instabilities.

## 5. Conclusions

In the present paper, numerical simulations of the flow in the diffuser of a wind tunnel were presented and discussed. It was shown that it is possible to build a very short and efficient diffuser, but that design and building of the device can be quite sensitive to fluid dynamical phenomena. A global instability can develop in the outflow region, leading to unsteady functioning of the test rig as a whole. Such problems can be avoided with a careful positioning of the elements composing the diffuser. This work also shows the utility of CFD in the design phase of test rigs; indeed, such simulations allowed to define correctly the technical constraints for the wind tunnel building. During next winter, the device will be actually built; tests performed on it will be compared to results of the present work to confirm them.

## Acknowledgment

The work described in the present paper was funded by INRIM. The authors wish to thank Mr. F. Alasia for his help in the preparation of the CAD models used in the definition of the geometry. Thanks also go to Dr. D. Camatti (DIASP-PoliTO) and Mr. I. Cozza (graduate student, DIASP-PoliTO) for useful comments and discussion about the simulations.

## References

[1] Barlow J. B., Rae W. H. Jr. and Pope A. *Low-Speed Wind Tunnel Testing (III edition)* John Wiley & Sons, inc., New York (U.S.A.), 1999

[2] Ferrari, C. *Rendiconti Sperimentali del Laboratorio di Aeronautica del R. Istituto Superiore di Ingegneria di Torino - 1a Serie – Determinazione della Caratteristiche della Galleria del Vento*. L'Aerotecnica – V. XIV – N. 4 – April 1934.

[3] Panetti, M. *Venticinque anni di attività del laboratorio di aeronautica al Politecnico di Torino*, Estratto dalla Rassegna Mensile Municipale "Torino" – N. 9 – September 1937.

[4] Piccato A., Malvano R. and Spazzini P.G. *Metrological features of the rotating low-speed anemometer calibration facility at INRIM.* Metrologia 47(1), pp. 47-57, 2010

[5] Piccato A., Spazzini P.G. and Malvano R. *Mapping of flow features in a wind tunnel*. In Proceedings of the 7th ISFFM Symposium, Anchorage, Alaska (U.S.A.), 2009.

[6] Spazzini P.G., Piccato A. and Malvano R. *Metrological features of the linear low-speed anemometer calibration facility at I.N.RI.M.* Metrologia 46(1), pp. 109-118, 2009

[7] CD-ADAPCO *STAR-CCM+ version 3.02.003 User Manual*, 2008